Biosensors and Bioelectronics 142 (2019) 111499

Contents lists available at ScienceDirect

Biosensors and Bioelectronics

journal homepage: www.elsevier.com/locate/bios

A close-packed imprinted colloidal array for naked-eye detection of glycoproteins under physiological pH

Wei Chen*, Min Fu, Xixi Zhu, Qingyun Liu**

College of Chemical and Environmental Engineering, Shandong University of Science and Technology, Qingdao, Shandong, 266590, China

ARTICLE INFO

Keywords:
Colloidal array
Glycoprotein
Molecular imprinting technology
Biosensors

ABSTRACT

According to the combination of colloidal crystals and molecular imprinting techniques, a novel close-packed imprinted colloidal array (CPICA) for naked-eye horseradish peroxidase (HRP) detection at physiological pH was proposed. The CPICA was fabricated by self-assemble of monodispersed HRP imprinted particles. The HRP imprinted particles were prepared based on surface imprinting technique and immobilized template strategy using 2,4-difluoro-3-formylphenylboronic acid (DFFPBA) as functional monomer which allowed the material binding of HRP at physiological pH (denoted as SiO_2@DFFPBA/MIPs). The adsorption capacity of the SiO_2@DFFPBA/MIPs for HRP was 1.16 μmol/g, and reached saturated adsorption within 25 min. The limit of detection (LOD) of the CPICA was 3.0×10^{-13} mol/mL. In addition, the adsorption of HRP on the CPICA could be directly transferred into visible color changes and readable optical signals through the reflection peak shifts. The structure color of the CPICA changed from brilliant blue to dark red with an maximum red shift of 87 nm when the HRP concentration increased from 2.5 to 20.0 μmol/L. Moreover, the CPICA could be used to detect HRP from human serum sample, which demonstrated the promising application prospects in colorimetric sensors.

1. Introduction

Glycoproteins play significant roles in various biological process, such as molecular recognition, immune response, blood coagulation, and so on. Numerous studies have proven that the content of glycoprotein in physiological fluids provide valuable information for disease diagnosis and therapy (Kubo et al., 2017; Saeki et al., 2019). Considerable efforts have been devoted to develop effective methods for detection of glycoproteins from complex biological samples, including gas chromatography (GC), high-pressure liquid chromatography (HPLC), and enzyme linked immunosorbent assay (ELISA)(Kishino and Miyazaki, 1997). Although these methods have achieved success in sensitivity and specificity for the detection of glycoproteins, they suffer from time consuming, sophisticated equipment and expensive. Thereby, an easy-to-operate, low-cost and efficient approach to detect glycoproteins is still urgently needed.

Recently, colloidal crystals have been widely used as diversified chemo/biosensors owing to its fascinating optical properties and bright structural color derived from periodic variation in the refractive index (Lee et al., 2017). Particularly, if the building blocks of the colloidal crystals are responsive polymer hydrogels, they may swell or shrink in response to environmental conditions, which lead to changes in optical properties, accompany by visually structure color changes (Aguirre et al., 2010; Kim et al., 2018). On this basis, various molecular recognition elements and stimuli responsive units have been introduced into the colloidal crystals to develop self-reporting sensors for detection of pH (Shin et al., 2012), proteins (Chen et al., 2017), glucose (Kim et al., 2019) and diols (Couturier et al., 2016) et al.

On the other hands, molecular imprinting is a facile technique for fabrication of molecularly imprinted polymers (MIPs) with specific nanocavities which are complementary in shape and functionality to the target molecules (Pan et al., 2017; Wang et al., 2016b). The MIPs with favorable binding affinity and specificity toward the imprinted molecules can act as artificial antibodies (Pan et al., 2018). In this respect, the combination of colloidal crystals and molecule imprinting technique could improve the specificity of traditional colloidal crystal sensors, owing to the recognition sites which are formed during imprinting process (Wang et al., 2018). More to the point, the molecular recognition events of the imprinted nanocavities will provide a readable optical signal through a change in reflection peak derived from the highly ordered structure of the colloidal crystals. Simultaneously, the accompanied change in structure color is visible, which makes it promising in naked-eye detection(Gam et al., 2017). Since the concept of combining photonic crystals with molecular imprinting proposed by Li's

* Corresponding author.
** Corresponding author.
E-mail addresses: chenwei30012@163.com (W. Chen), qyliusdu@163.com (Q. Liu).

https://doi.org/10.1016/j.bios.2019.111499
Received 24 May 2019; Received in revised form 9 July 2019; Accepted 10 July 2019
Available online 10 July 2019
0956-5663/

group, the feasibility of this approach have been proved by many groups. For instance, Li and coworkers proposed a general method for the synthesis of molecularly imprinted films with inverse opal structure for specific recognition of amino acid (Hu et al., 2006), protein (Hu et al., 2007) and atrazine (Wu et al., 2008). Gu et al. fabricated a molecularly imprinted polymer bead with photonic crystal structure, for the label-free detection of biomolecules (Wang et al., 2016a). Meng et al. reported several imprinted photonic crystal hydrogels for sensing glucose (Xue et al., 2014) and explosive (Lu et al., 2016). Griffete et al. prepared three-dimensional imprinted macroporous array for pH sensing (Griffete et al., 2012) and bisphenol A detection (Griffete et al., 2011). These imprinted films with inverse opal structure exhibit satisfactory specificity and fast response. However, the preparation process of the special film is complicated, especially the removal of template array from the hydrogel after polymerization may destroy the 3D ordered structure.

It is well known that phenylboronic acid (PBA) can bind to cis-diol-containing compounds when the environmental pH is ≥ the pK_a of the boronic acid, according to the formation of reversible five-membered or six-membered ester ring. Whereas the complexes become dissociable when environmental pH is < the pK_a of the boronic acid (Preinerstorfer et al., 2009). Recently, phenylboronic acid have been widely used as functional monomers in preparation of MIPs for specific glycoproteins detection, and become a powerful tool for glycosides research. However, most boronic acid-functionalized MIPs can bound to glycoproteins only within alkaline pH range, which may result in denaturation of the glycoproteins (Kajisa and Sakata, 2018). Therefore, one of the greatest challenge in the development of boronic acid-functionalized MIPs is how to achieve the binding event at physiological pH.

In this paper, a close-packed imprinted colloidal array (CPICA) for naked-eye HRP detection was developed by combination of colloidal crystals and molecular imprinting techniques. First, the monodispersed SiO_2@DFFPBA/MIPs were prepared using DFFPBA as affinity ligands, the two electron-withdrawing groups on the benzene ring rendered the lower pK_a value of the PBA, leading to binding of the glycoprotein at physiological pH. Secondly, the SiO_2@DFFPBA/MIPs was self assembled into CPICA via a vertical deposition method. Compared with the inverse opal structure, the preparation process of the CPICA is simple without using opal as template which have to be removed after the polymerization process. Finally, the adsorption of HRP on the CPICA could be directly transferred into visible color changes and readable optical signals through the reflection peak shifts.

2. Experimental section

2.1. Materials

Tetraethyl orthosilicate (TEOS), (3-Aminopropyl) triethoxysilane (APTES), Sodium cyanotrihydridoborate and 2,4-Difluoro-3-formylphenylboronic acid (DFFPBA) were bought from Sigma-Aldrich. Ethanol, methanol, toluene and ammonia solution (25–28%) were provided by Chengdu kelong Chemical Reagent Co., Ltd. Ammonium persulphate (APS), methylene-bis-acrylamide (Bis), N, N, N′, N′-tetramethylenediamine (TEMED), horseradish peroxidase (HRP), bovine serum albumin (BSA), ribonuclease A (RNase A), ribonuclease B (RNase B), transferrin (TRF), ovalbumin (OVA) and lysozyme (Lys) were all purchased from Shanghai Aladdin Bio-Chem Technology Co., Ltd.

2.2. Instrumentation

The reflection of the imprinted colloidal array was recorded by an FX2000-EX spectrometer with an HL2000 light source and an FIB-Y-400-L (2)-TA-DUV Y type optical fiber (Shanghai Fuxiang Optics Co., Ltd.). The scanning electron microscopy (SEM) was performed with a APREO scanning electron microscope (FEI, USA). Transmission electron microscopy (TEM) was conducted by a JEM-2100 microscope.

2.3. Preparation of DFFPBA modified SiO_2 nanoparticles (SiO_2@ DFFPBA)

The detailed synthetic procedure of monodispersed silica nanoparticles referred to our previous works (Chen et al. 2017, 2019). The obtained silica nanoparticles were orderly modified with APTES and DFFPBA to produce DFFPBA-functionalized silica nanoparticles (denoted as SiO_2@DFFPBA). In brief, 1 g silica nanoparticles were added to 80 mL anhydrous toluene in a 250 mL flask and dispersed thoroughly by ultrasound. Then, a mixture of APTES and anhydrous toluene was added dropwise into the above solution with continuously stirring at 90 °C. After reaction for 12 h, the amino functionalized silica nanoparticles (SiO_2@NH_2) were cleaned by acetone and ethanol several times, followed by drying at 45 °C in vacuum oven overnight. Then, 1.0 g dried SiO_2@NH_2, 800 mg DFFPBA and 800 mg sodium cyanoborohydride ($NaBH_3CN$) were dispersed into 150 mL methanol by ultrasound. The obtained mixture was stirred at room temperature for 12 h. The resulting boronic acid functionalized silica nanoparticles (SiO_2@DFFPBA) was separated via centrifugation, washed by deionized water and ethanol for several times, and dried at 45 °C in a vacuum oven overnight.

2.4. Preparation of HRP-imprinted polymers (SiO_2@DFFPBA/MIPs)

The SiO_2@DFFPBA/MIPs composites with HRP as the template glycoprotein were synthesized according to the boronate affinity oriented surface imprinting approach. Typically, 400 mg SiO_2@DFFPBA nanospheres was dispersed in 100 mL PBS (15 mmol/L, pH = 7.4) by ultrasonication. Then 80 mg HRP was added to the suspension and shaken at room temperature for 3 h, the mixture was shaken at room temperature for 2.5 h for the immobilization of HRP on SiO_2@DFFPBA surface via the formation of covalent cyclic ester. Sequentially, 100 mg AAm and 2.0 mg Bis were added to the above solution, after 2 h shaking for preassembly, the mixture was purged with nitrogen gas for 45 min. Followed by the addition of 30 mg KPS solution and 15 μL TEMED, polymerization was carried out and continued under stirring at room temperature for 24 h. The HRP-imprinted polymers (SiO_2@DFFPBA/MIPs) was collected by centrifugation and washed with PBS three times to remove unreacted monomers. Finally, the SiO_2@DFFPBA/MIPs were washed with acetic acid/aqueous (2/8, v/v) solutions to remove the embedded template molecules. The obtained product was washed by water and ethanol for several times and dried for further use. The non-imprinted polymer (SiO_2@DFFPBA/NIPs) were prepared using the same procedure without adding the template in the polymerization mixture.

2.5. Binding properties of SiO_2@DFFPBA/MIPs and SiO_2@DFFPBA/NIPs

The kinetics adsorption experiments were carried out as follows: 10 mg SiO_2@DFFPBA/MIPs (or SiO_2@DFFPBA/NIPs) was incubated with 1 mL HRP solutions (15 μmol/L, pH 7.4) for different interval time (5–40 min) at room temperature. Afterwards, the SiO_2@DFFPBA/MIPs were separated by centrifugation. The HRP concentration in the supernatant was determined by UV spectrometer. And the adsorption capacity (Q mg/g) of the SiO_2@DFFPBA/MIPs for HRP was figured out by formula (1):

$$Q = (C_0 - C_f)V/m \quad (1)$$

Where C_0 (μmol/L) represents the initial concentration of HRP solution, C_f (μmol/L) represents the residue concentration of HRP in the supernatant, V (L) is the adsorption mixture volume, and m (g) stands for the quantity of SiO_2@DFFPBA/MIPs.

The isothermal adsorption experiments were performed out similarly to the kinetics adsorption experiments. The initial concentration of HRP solutions changed from 1.0 to 25 μmol/L. The adsorption time was kept constant at 25 min.

The selectivity of the SiO_2@DFFPBA/MIPs and SiO_2@DFFPBA/NIPs was also studied via comparing the amount of different proteins adsorbed on the SiO_2@DFFPBA/MIPs and SiO_2@DFFPBA/NIPs. The initial concentration of each protein was 15 μmol/L, and the adsorption time was kept at 25 min.

2.6. Fabrication of the CPICA and CPNCA

The CPICA was fabricated via a vertical deposition method. The glass slides were immersed in a H_2SO_4/H_2O_2 (7/3, v/v) solution for 24 h and then rinsed with deionized water before use. The SiO_2@DFFPBA/MIPs were dispersed in deionized water (0.25 wt%) and stored in an open glass beaker in which a glass slide was immersed vertically. The SiO_2@DFFPBA/MIPs solution was put inside an incubator at 30 °C with humidity of 40%. As the dispersion evaporated, the monodispersed SiO_2@DFFPBA/MIPs deposited on both sides of the glass slides, and highly ordered CPICA was formed.

The CPNCA was synthesized by the same procedure with CPICA, employing SiO_2@DFFPBA/NIPs as building blocks instead of SiO_2@DFFPBA/MIPs.

2.7. Sensing properties of the CPICA

To investigate the sensing properties of the CPICA to the target protein, the CPICA was cut into small pieces (10 × 5 mm) and equilibrated in 10 mL PBS buffer (15 mmol/L, pH = 7.4) before use. Then the CPICA was immersed into 5 mL HRP solutions (the initial concentration ranging from 2.5 to 25.0 μmol/L) for 25 min. The reflection spectra of the CPICA were recorded by spectrometer with the fiber probe fixed vertically above the CPICA surface. Photographs of the CPICA were taken by a digital camera.

3. Results and discussion

3.1. Preparation and characterization of the SiO_2@DFFPBA/MIPs

The principle and the procedure of the preparation process were illustrated in Fig. 1. Firstly, the silica nanoparticles were prepared by modified Stöber method and reacted with APTES to get amino functionalized SiO_2 (SiO_2@NH_2). Secondly, DFFPBA was covalently immobilized onto the surface of SiO_2@NH_2 via imine bonds formation between the aldehyde groups of DFFPBA and amino groups on SiO_2@NH_2. Thirdly, HRP, a glycoprotein which was choosen as template molecule, was immobilized onto the DFFPBA-grafted beads (SiO_2@DFFPBA) surface through the formation of cyclic ester between the boronate acid and the cis-diol group of HRP. Then, AAm and Bis was added as functional monomer and cross-linker respectively. After polymerization, a polymeric network around SiO_2@DFFPBA and HRP complex was produced. Finally, the SiO_2@DFFPBA/MIPs with recognition sites were obtained after the removal of the embedded templates.

The morphological structures of SiO_2 and SiO_2@DFFPBA/MIPs were studied by SEM and TEM. The uniform and sphere-shaped SiO_2 nanoparticles with smooth surface were observed from Fig. S1a. The diameter of the SiO_2 nanoparticles were ~300 nm. In contrast, the surface of the SiO_2@DFFPBA/MIPs was rough after surface imprinted polymerization (Fig. S1b), indicating the deposition of polymer layer. From the TEM images of the SiO_2 and SiO_2@DFFPBA/MIPs (Figure S1c and 2d), asemitransparent polymer shell was presented on the surface of SiO_2@DFFPBA/MIPs and the shell thickness was estimated to be 20 nm. Despite of the rough surface, the coreshell SiO_2@DFFPBA/MIPs still possessed good dispersibility and relatively uniform size, implying that the SiO_2@DFFPBA/MIPs were highly advantageous for assembling into close-packed colloidal array.

3.2. Selectivity of the SiO_2@DFFPBA

The selectivity of the SiO_2@DFFPBA/MIPs was investigated to confirm the immobilization of boronic acid functional group on the SiO_2@NH_2, which was a key step for the oriented surface imprinting technology. As we known, the boronic acid groups can form covalent complexes with cis-diol-containing compounds when the surrounding pH value was above the pKa value of the boronic acid. In this experiment, four glycoproteins (HRP, TRF, RNase B and OVA) was choosen as cis-diol-containing compounds, while two non-glycoproteins (RNase A and BSA) was used as non-cis-diol-containing compounds. As depicted in Fig. S2, under neutral pH conditions, the amount of the glycoproteins captured by SiO_2@DFFPBA/MIPs were all much higher than that of the non-glycoproteins. This implies that the DFFPBA was grafted on the surface of the SiO_2@NH_2. Moreover, the result was in line with the previous studies that the DFFPBA-functionalized materials exhibited good selectivity to glycoproteins under neutral pH (Li et al., 2018).

3.3. Optimizing the polymerization conditions and binding pH

As mentioned in previous report, crosslinking degree was an important factor which affected the recognition behavior of the imprinted materials (Gao et al., 2013). A series of SiO_2@DFFPBA/MIPs and SiO_2@DFFPBA/NIPs were prepared with different molar ratios of the functional monomer (AAm) and crosslinker (Bis), and their adsorption performances were investigated. As displayed in Fig. S3, both binding capacity and imprinting factors of the SiO_2@DFFPBA/MIPs increased with the increasing crosslinking degree firstly, and achieved maximum at the amount of 4.0% Bis, followed by a decline. Based on the above results, it was inferred that the SiO_2@DFFPBA/MIPs with lower crosslinking degree were too soft to maintain the shape of the imprinted molecules in the polymer backbone after template removal. The spatial fluctuations in the imprinted cavities caused the diminished binding capacity. As the crosslinking degree increased, more effective imprinted cavities were obtained in SiO_2@DFFPBA/MIPs, resulting in the increasing of the adsorption capacity. However, it was difficult for protein removal and rebinding in the highly crosslinked imprinted material owing to the strong steric hindrance. Therefore, the SiO_2@DFFPBA/MIPs at the amount of 4.0% Bis was an optimum crosslinking degree that provided satisfactory recognition performance.

The pH value is a crucial factor that influence the interaction between the boronic acid and glycoprotein. In order to detect HRP under physiological pH, DFFPBA (pK_a = 6.5) was chosen as boronicacid affinity ligand to prepare the imprinted materials (Cheng et al., 2015). The electron-withdrawing effect of the fluorine atoms of benzene ring contributed to lower pK_a value of phenylboronic acid. Fig. S4 presented the effect of pH on the binding behavior of the SiO_2@DFFPBA/MIPs and SiO_2@DFFPBA/NIPs. The adsorption capacity and the imprinting factor of SiO_2@DFFPBA/MIPs to HRP increased significantly with the increasing pH value, and reached a maximum at pH 7.4. Such a binding pH was lower than the most reported boronate affinity materials, which usually used 3-aminophenylboronic acid (APBA) and 4-vinylphenylboronic acid (VPBA) as boronic acid monomers. This result confirmed that the SiO_2@DFFPBA/MIPs was promising for detection of glycoprotein under physiological pH. It is noteworthy that the adsorption capacity of SiO_2@DFFPBA/MIPs to HRP decreased at pH 9.0, possibly due to the decrease in activity of HRP under alkaline condition.

3.4. Binding properties of SiO_2@DFFPBA/MIPs and SiO_2@DFFPBA/NIPs

3.4.1. Adsorption isotherms

In order to determine the binding capacity of the SiO_2@DFFPBA/MIPs and SiO_2@DFFPBA/NIPs, saturation adsorption experiments were performed at different initial concentrations of HRP. According to Fig. 2a, the amount of HRP bound to SiO_2@DFFPBA/MIPs increased rapidly as the concentrations of HRP increased from 1.0 to 10.0 μmol/L,

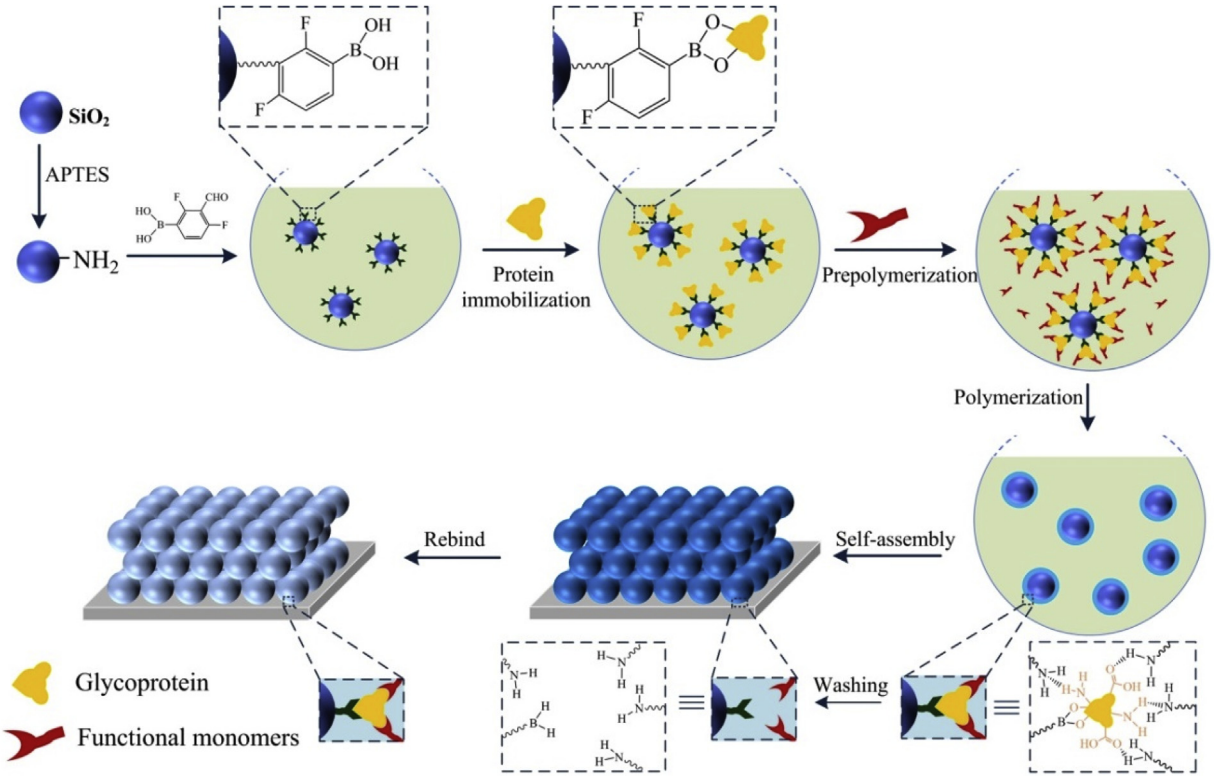

Fig. 1. Schematic illustration of preparation procedure of the CPICA.

and reached an adsorption plateau at 15 μmol/L. The maximum adsorption capacity of SiO_2@DFFPBA/MIPs and SiO_2@DFFPBA/NIPs were 1.16 μmol/g and 0.67 μmol/g, respectively. The great gap between the binding capacity of SiO_2@DFFPBA/MIPs and SiO_2@DFFPBA/NIPs implied the formation of specific recognition sites during the imprinting process.

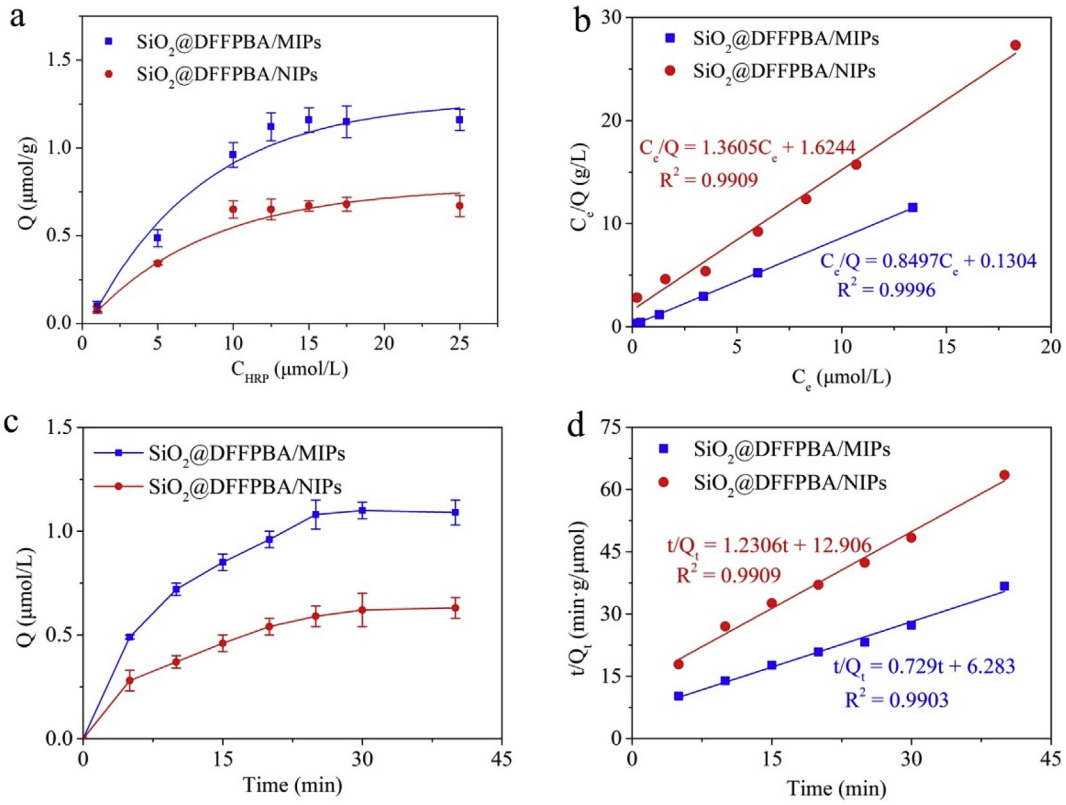

Fig. 2. The adsorption isotherms (a), scatchard plot (b), adsorption kinetics (c) and Pseudo-second-order model (d) of the SiO_2@DFFPBA/MIPs and SiO_2@DFFPBA/NIPs.

To further understand the binding behavior of SiO_2@DFFPBA/MIPs and SiO_2@DFFPBA/NIPs, Langmuir isotherm model was adopted to describe the saturation adsorption data, which can be expressed as (Gao et al., 2016):

$$\frac{C_e}{Q_e} = \frac{1}{K_m Q_m} + \frac{C_e}{Q_m} \quad (2)$$

Where C_e (μmol/L) represents the equilibrium concentration of HRP in supernatant, Q_m (μmol/g) and K_m (L/μmol) are the theoretical maximum adsorption capacity and Langmuir adsorption equilibrium constant, respectively.

Fig. 2b showed Scatchard plot of the adsorption experiment. According to liner regression equations, the Q_m and K_m of SiO_2@DFFPBA/MIPs and SiO_2@DFFPBA/NIPs were calculated and listed in Table S1. The adsorption isotherms of SiO_2@DFFPBA/MIPs and SiO_2@DFFPBA/NIPs to HRP agreed well with Langmuir isotherm model with $R^2 > 0.99$. It was worth mentioning that the maximum adsorption capacity (SiO_2@DFFPBA/MIPs: 1.16 μmol/g, SiO_2@DFFPBA/NIPs: 0.67 μmol/g) obtained from experimental results accorded well with the theoretical maximum adsorption capacity (SiO_2@DFFPBA/MIPs: 1.18 μmol/g, SiO_2@DFFPBA/NIPs: 0.74 μmol/g) calculated by Langmuir isotherm model. It can be inferred that the adsorption of HRP onto SiO_2@DFFPBA/MIPs and SiO_2@DFFPBA/NIPs was monolayer binding.

3.4.2. Adsorption kinetics

The adsorption kinetics curves of HRP onto SiO_2@DFFPBA/MIPs and SiO_2@DFFPBA/NIPs are investigated and displayed in Fig. 2c. The amount of HRP adsorbed on SiO_2@DFFPBA/MIPs and SiO_2@DFFPBA/NIPs increased sharply in the first 10 min, and became constant when the incubation time was more than 25 min. The thin imprinted layer facilitated the fast transfer rate of the SiO_2@DFFPBA/MIPs. Whereas the SiO_2@DFFPBA/NIPs needed more time to reach the adsorption equilibrium. Possibly due to the random distribution of functional groups without imprinting process, and the adsorption of HRP on the SiO_2@DFFPBA/NIPs was mainly contributed by non-specific binding.

The kinetic data were analyzed by pseudo second-order rate equation to investigate the adsorption kinetic mechanism, which can be described as (Gao et al., 2016):

$$\frac{t}{Q_t} = \frac{1}{K_2 {Q_e}^2} + \frac{t}{Q_e} = \frac{1}{v_0} + \frac{t}{Q_e} \quad (3)$$

Where Q_e and Q_t (μmol/g) are the binding capacities of the SiO_2@DFFPBA/MIPs and SiO_2@DFFPBA/NIPs at equilibrium and time t, respectively. K_2 (g/μmol·min) represents the rate constant of pseudo-second-order adsorption, v_0 (μmol/g·min) stands for the initial adsorption rate.

As depicted in Fig. 2d and Table S2, the adsorption data followed the pseudo-second-order model quite well with $R^2 > 0.99$. It was obvious that the v_0 of the SiO_2@DFFPBA/MIPs (0.159 μmol/g·min) was higher than that of the SiO_2@DFFPBA/NIPs (0.077 μmol/g·min). This result further confirmed the fast transfer rate of the HRP on the SiO_2@DFFPBA/MIPs.

3.4.3. Adsorption specificity

To investigate the specificity of SiO_2@DFFPBA/MIPs for HRP (Mw 44 kDa, pI 7.2), six types of proteins with different molecular weights and isoelectric point were used including TRF (Mw 80 kDa, pI 5.5), OVA (Mw 45 kDa, pI 4.7), BSA (Mw 68 kDa, pI 4.6), Hb (Mw 64.5 kDa, pI 6.8–7.0), Lys (Mw 14.4 kDa, pI 10.7) and Cyt C (Mr 12.4, pI 10.2). Fig. S5 displayed the binding capacity of the SiO_2@DFFPBA/MIPs and SiO_2@DFFPBA/NIPs for these proteins with initial concentration of 15 μmol/L. It was obvious that the amount of HRP bound to the SiO_2@DFFPBA/MIPs was much higher than that of other proteins. The binding capacity of SiO_2@DFFPBA/MIPs to HRP was also higher than that of SiO_2@DFFPBA/NIPs. The result suggested that imprinting sites complementary to HRP were formed during the imprinting process, and a small amount of the reference proteins were bound to SiO_2@DFFPBA/MIPs and SiO_2@DFFPBA/NIPs owing to nonspecific adsorption. The specificity of SiO_2@DFFPBA/MIPs for HRP further proved that imprinted material was promising for HRP detection.

To further demonstrate the selectivity, the SiO_2@DFFPBA/MIPs was used to separate HRP from human serum sample. The human serum sample was diluted 50-fold with PBS (15 mmol/L, pH = 7.4). As shown in Fig. S6, the noticeable peak appeared around 280 nm in the UV–vis spectrum of diluted human serum sample, indicating the existence of other constituent. The peak of HRP at 403 nm can be observed after the human serum spiked with 10 μmol/L HRP. When the mixture was incubated with SiO_2@DFFPBA/MIPs, HRP were detected in the elution. While the peak at 280 nm was not observed from the elution, indicating the other constituent of the human serum was not separated by the SiO_2@DFFPBA/MIPs. The result confirmed the outstanding selectivity of SiO_2@DFFPBA/MIPs to HRP.

3.5. Fabrication and characterization of the CPICA

The monodispersed SiO_2@DFFPBA/MIPs were self-assembled into 3D colloidal array on the surface of glass slides via vertical deposition method. Concretely, a clean microscopy slide (size: 24 mm*50 mm) was vertically placed into a vial containing SiO_2@DFFPBA/MIPs aqueous solution. A meniscus region was formed during the evaporative driven self-assembly process, and the water evaporated out of the thin meniscus, leading to the assembly of the SiO_2@DFFPBA/MIPs(N et al., 1992; P et al., 1999). Fig. 3 showed the SEM images and structure color of the obtained CPICA. A highly ordered close-packed 3D array was clearly observed, and no crack was appeared on the top-view SEM image of the CPICA in a large area (Fig. 3a and b). The thickness of the CPICA was around 7 μm from the cross-section SEM image (Fig. 3c). Meanwhile, as shown in Fig. 3d, the structure color of the CPICA was brilliant blue, owing to the Bragg diffraction of visible light on the highly-ordered periodical 3D structures.

3.6. Sensing properties of the CPICA

The experimental procedures for characterizing the sensing properties of CPICA was shown in Fig. 4. Generally, the CPICA was cut into small pieces (10 × 5 mm) and equilibrated in 10 mL PBS buffer before use. Then the CPICA was immersed into different solutions for 25 min. The reflection spectra of the CPICA were recorded by spectrometer with the fiber probe fixed vertically above the CPICA surface.

3.6.1. Effect of metal ions

The influence of metal ions and ionic strength (NaCl, $FeCl_3$, $MgCl_2$) on the obtained CPICA was investigated by varying concentrations of NaCl, $FeCl_3$ and $MgCl_2$ in PBS. As shown in Fig. S7, the CPICA exhibited slight red shifts in different NaCl solutions, while no wavelength shift was observed when the CPICA responded to $FeCl_3$ and $MgCl_2$. Therefore, the effect of ion strength and metal ions were negligible.

3.6.2. Response of the CPICA to HRP

The sensing properties of the CPICA to different concentrations of HRP in PBS were investigated. As displayed in Fig. 5, the reflection peak of CPICA is sensitive to the rebinding of HRP. When the concentrations of HRP increased from 0 to 25 μmol/L, the reflection peak of the CPICA red shifted 87 nm from 683 nm to 770 nm, accompanied with an evident change in the “structure color”. The insert images in Fig. 5a presented the different CPICA colors before and after HRP detection. Gradual color change from brilliant blue, through green, yellow to dark red with increasing HRP concentrations could be easily distinguished by the naked eye. In contrast, the red shift of the CPNCA reached the maximum of 35 nm in response to HRP, and the structure color of the CPNCA maintained brilliant blue with the concentration of the HRP up to 10 μmol/L (Fig. 5b). Moreover, as seen from Fig. 5d, the red shift of

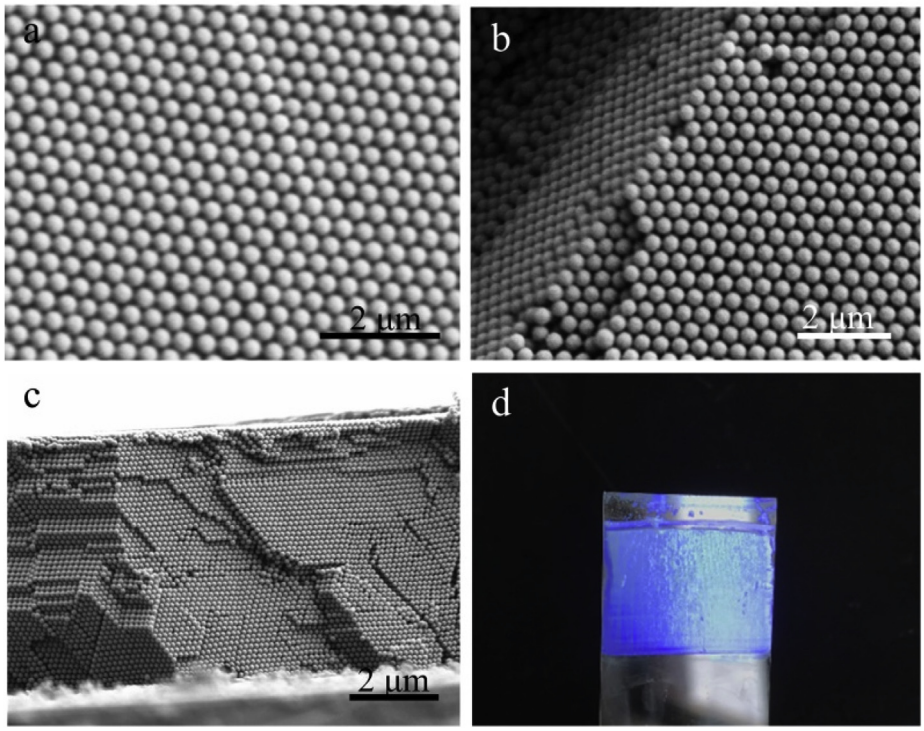

Fig. 3. Top view (a, b) and cross-section (c) SEM images of the CPICA, (d) photograph of the CPICA.

the CPICA in response to HRP was much higher than that of CPNCA, and became constant when the HRP concentration was higher than 20 μmol/L. As a control, silica colloidal array was also synthesized, and its red shift was only 5 nm in response to 25.0 μmol/L HRP (Fig. 5c).

The red-shift of the CPICA reflection peak and the change in structure colors in response to different HRP solutions could be explained by Bragg's Law(Fenzl et al., 2014):

$$m\lambda_{max} = 2nd\sin\theta \quad (4)$$

Where λ_{max} is the wavelength of the reflection peak, d represents the average lattice spacing of the colloidal array, n stands for the refractive index of the system, m is the order of the Bragg diffraction, and θ represents the angle between the incident light and colloidal array surface. The value of θ was set to be 90° in our experiment.

When the CPICA was incubated with HRP solutions, HRP bound to the recognition sites of the polymer network on the silica surface which was formed during the imprinting process. According to formula (4), the swelling of the SiO_2@DFFPBA/MIPs and changes in refractive index resulted from the adsorption of HRP on the CPICA, leading to the red shift of reflection peak accompanied by visual color change. The red shift in the reflection peak of CPNCA probably due to non-specific adsorption, as amino groups and phenylboronic acid groups were embedded in the SiO_2@DFFPBA/NIPs.

Of particular note, Table S3 listed HRP concentrations corresponding to different colors and reflection peak shifts. The reflection peak of the CPICA red shifted in response to HRP, the exact concentration of HRP can be obtained by the red shift of the CPICA. While the HRP concentrations could be roughly estimated from the structure color of the CPICA. For instance, the when the CPICA turned green, the concentration of HRP was ~7.5 μmol/L.

The limit of detection (LOD) of this CPICA sensor to HRP was calculated to be 3.0×10^{-13} mol/mL, by assuming a minimum instrument

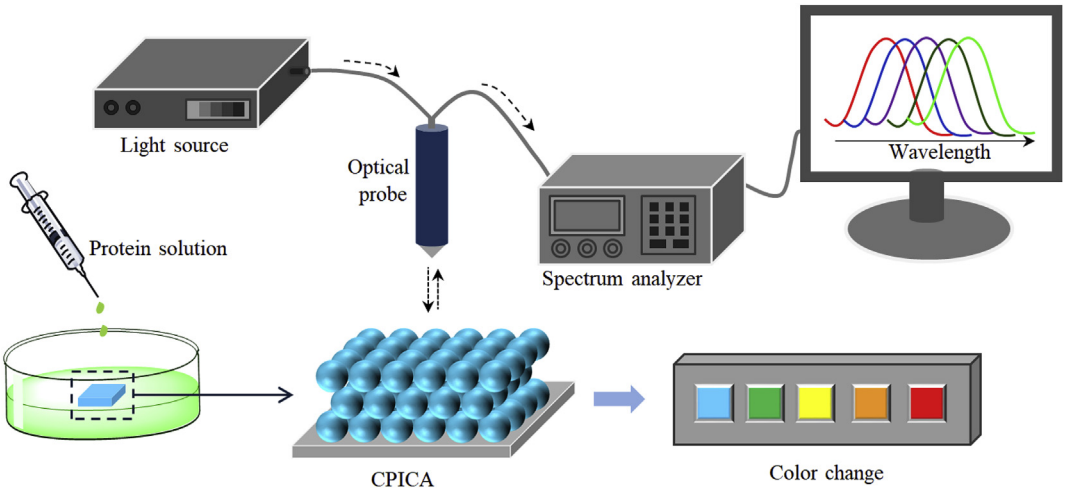

Fig. 4. Experimental procedures for characterizing the sensing properties of CPICA.

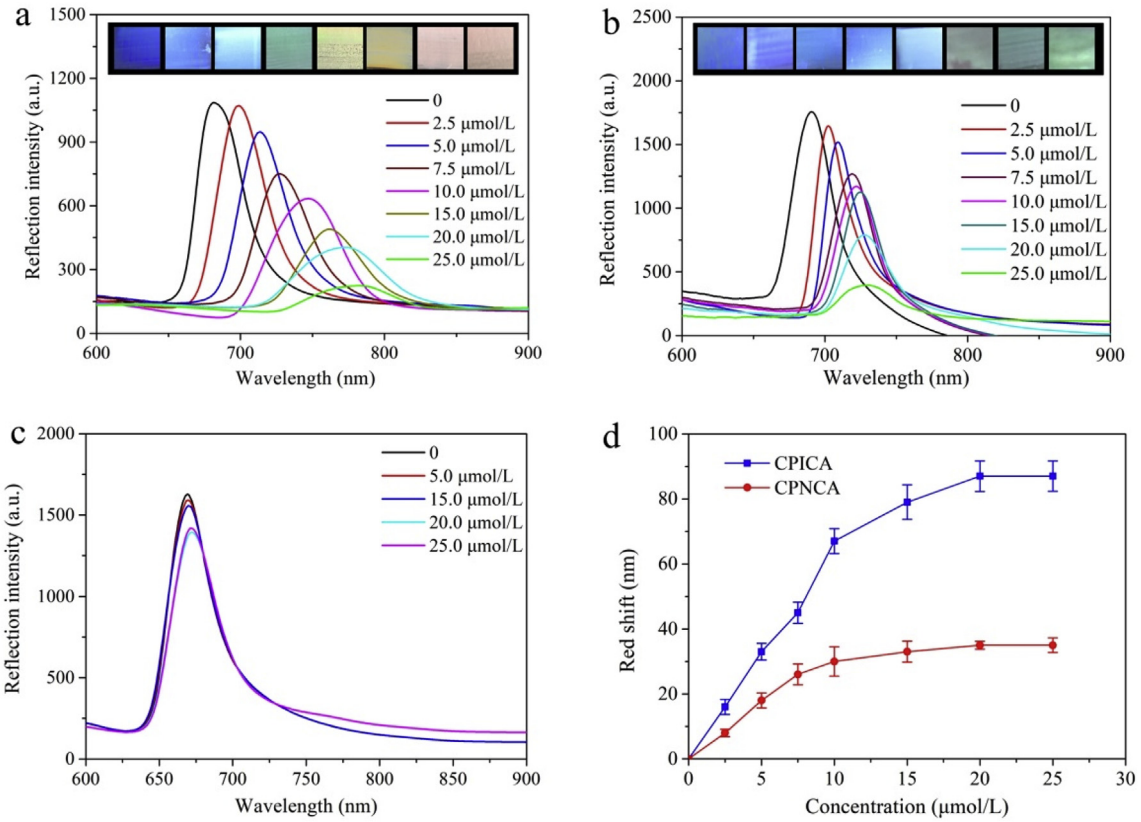

Fig. 5. Optical responses of CPICA (a), CPNCA (b) and silica array (c) to various concentrations of HRP. (d) Plots of red shifts of CPICA and CPNCA in response to different HRP concentrations. (For interpretation of the references to color in this figure legend, the reader is referred to the Web version of this article.)

detectable reflection shift of 0.5 nm. To evaluate the sensitivity of CPICA, a table was provided to compare the LOD of this method with others (Table S4). Although the LOD of this method was not prominent, the novel CPICA was easy to prepare and could construct a simple detection device, which could render the visual detection.

3.6.3. Selectivity of the CPICA

To evaluate the selectivity of the CPICA, we incubated the CPICA in PBS solutions containing 20 μmol/L Lys, OVA, TRF and BSA, respectively. The optical responses of CPICA and CPNCA to these proteins were depicted in Fig. 6. The response of the CPICA to HRP was much higher than that of the other proteins, owing to the recognition sites complementary to the HRP on the surface of the silica particles of the CPICA. Unlike the CPICA, without the tailor-made binding sites, small amount of protein was bound to the surface of CPNCA, leading to slight red shift of the reflection peak. The result proved that the CPICA had good specificity to HRP.

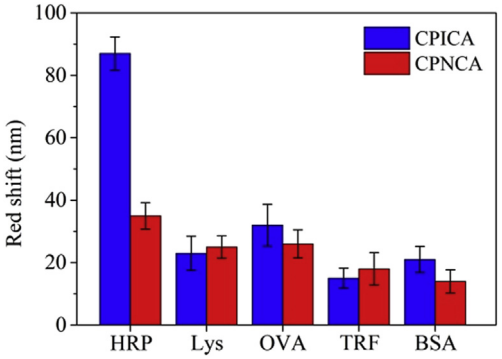

Fig. 6. Optical responses of CPICA and CPNCA to different proteins.

3.6.4. Reversibility of response of the CPICA

The reversibility of response was one of the most essential properties of the biosensors in real application. Therefore, the reversibility of CPICA was evaluated by alternatively sensing HRP and then removed the HRP with 10 mL acetic acid/aqueous (2/8, v/v) solutions. Fig. S8 showed that the CPICA was reversible over three adsorption-regeneration cycles. The result implied that the obtained CPICA had good reproducibility without significant change in reflection wavelength.

3.6.5. Real sample analysis

In order to confirm the practical applicability, the CPICA was used to detect HRP from human serum sample. The human serum sample was diluted 50-fold with PBS (15 mmol/L, pH = 7.4), spiked with 10 μmol/L and 20 μmol/L HRP, respectively. The reflection spectra of the CPICA were recorded after soaked in the mixture for 25 min. As shown in Fig. S9, the CPICA exhibited slight red shifts in human serum sample, probably due to the existence of other constituent absorbed on the CPICA. While a significant red-shift was observed when CPICA was soaked in the spiked human serum samples. Therefore, the CPICA showed prospects in detecting HRP from biological samples.

4. Conclusions

In summary, a novel close-packed imprinted colloidal array (CPICA) for naked-eye HRP detection was developed by combination of colloidal crystals and molecular imprinting techniques. The CPICA exhibited satisfactory responsiveness to HRP at physiological pH, owing to DFFPBA with lower pK_a was chosen as boric acid affinity ligand during the imprinting process. The LOD of the CPICA was 3.0×10^{-13} mol/mL. The reflection peak of the CPICA red shifted 87 nm in response to 20.0 μmol/L HRP accompanied by structure color changing from brilliant blue to dark red. Besides, the good stability and selectivity

provided the promising applications of the CPICA in colorimetric sensors.

CRediT authorship contribution statement

Wei Chen: Conceptualization, Writing - original draft. **Min Fu:** Data curation. **Xixi Zhu:** Validation. **Qingyun Liu:** Writing - review & editing.

Acknowledgments

This work was supported by the National Natural Science Foundation of China (Grant No. 21805168), Natural Science Foundation of Shandong Province (Grant No. ZR2018BB046, ZR2017BB008), Scientific Research Foundation of Shandong University of Science and Technology for Recruited Talents (Grant No. 2017RCJJ040, 2017RCJJ041).

Appendix A. Supplementary data

Supplementary data to this article can be found online at https://doi.org/10.1016/j.bios.2019.111499.

Declaration of interest

The authors declare that they have no known competing financial interests or personal relationships that could have appeared to influence the work reported in this paper.

References

Aguirre, C.I., Reguera, E., Stein, A., 2010. Adv. Funct. Mater. 20 (16), 2565–2578.
Chen, W., Fu, M., Zhu, X., Liu, Q., 2019. Biosens. Bioelectron. 142. https://doi.org/10.1016/j.bios.2019.111492.
Chen, W., Shea, K.J., Xue, M., Qiu, L., Lan, Y., Meng, Z., 2017. Anal. Bioanal. Chem. 409 (22), 5319–5326.
Cheng, T., Li, H., Ma, Y., Liu, X., Zhang, H., 2015. Anal. Bioanal. Chem. 407 (12), 3525–3529.
Couturier, J., Wischerhoff, E., Bernin, R., Hettrich, C., Koetz, J., Sutterlin, M., Tiersch, B., Laschewsky, A., 2016. Langmuir 32 (17), 4333–4345.
Fenzl, C., Hirsch, T., Wolfbeis, O.S., 2014. Angew. Chem. Int. Ed. 53 (13), 3318–3335.
Gam, D., Bourdillon, C., Chaouche, S.L., Coolen, L., Maitre, A., Mangeney, C., Schwob, C., 2017. Angew. Chem. Int. Ed. 56 (33), 9710–9714.
Gao, F., Ma, X., He, X., Li, W., Zhang, Y., 2013. Colloids Surf., A 433, 191–199.
Gao, R., Hao, Y., Zhang, L., Cui, X., Liu, D., Zhang, M., Tang, Y., Zheng, Y., 2016. Chem. Eng. J. 284, 139–148.
Griffete, N., Frederich, H., Maitre, A., Ravaine, S., Chehimi, M.M., Mangeney, C., 2012. Langmuir 28 (1), 1005–1012.
Griffete, N., Frederich, H., Maitre, A., Schwob, C., Ravaine, S., Carbonnier, B., Chehimi, M.M., Mangeney, C., 2011. J. Colloid Interface Sci. 364 (1), 18–23.
Hu, X., An, Q., Li, G., Tao, S., Liu, J., 2006. Angew. Chem. Int. Ed. 45 (48), 8145–8148.
Hu, X., Li, G., Huang, J., Zhang, D., Qiu, Y., 2007. Adv. Mater. 19, 4327–4332.
Kajisa, T., Sakata, T., 2018. Acs Appl. Mater. Inter. 10 (41), 34983–34990.
Kim, D., Koh, Y.G., Lee, W., 2019. Phys. Status Solidi 13 (2), 1800416.
Kim, J., Lee, J., Kim, S., 2018. Adv. Mater. Interfaces 5 (10), 1701658.
Kishino, S., Miyazaki, K., 1997. J. Chromatogr. B 699 (1-2), 371–381.
Kubo, T., Furuta, H., Naito, T., Sano, T., Otsuka, K., 2017. Chem. Commun. 53 (53), 7290–7293.
Lee, S.S., Seo, H.J., Kim, Y.H., Kim, S.H., 2017. Adv. Mater. 29 (23), 1606894.
Li, D., Tu, T., Yang, M., Xu, C., 2018. Talanta 184, 316–324.
Lu, W., Asher, S.A., Meng, Z., Yan, Z., Xue, M., Qiu, L., Yi, D., 2016. J. Hazard Mater. 316, 87–93.
N, D., O, V., P, K., I, I., H, Y., K, N., 1992. Langmuir 8 (12), 3183–3190.
P, J., JF, B., KS, H., VL, C., 1999. Chem. Mater. 11 (8), 2132–2140.
Pan, G., Shinde, S., Yeung, S.Y., Jakstaite, M., Li, Q., Wingren, A.G., Sellergren, B., 2017. Angew. Chem. Int. Ed. 56 (50), 15959–15963.
Pan, J., Chen, W., Ma, Y., Pan, G., 2018. Chem. Soc. Rev. 47 (15), 5574–5587.
Preinerstorfer, B., Lammerhofer, M., Lindner, W., 2009. J. Sep. Sci. 32 (10), 1673–1685.
Saeki, T., Sunayama, H., Kitayama, Y., Takeuchi, T., 2019. Langmuir 35 (5), 1320–1326.
Shin, J., Han, S.G., Lee, W., 2012. Anal. Chim. Acta 752, 87–93.
Wang, H., Xu, Q., Shang, L., Wang, J., Rong, F., Gu, Z., Zhao, Y., 2016a. Chem. Commun. 52 (16), 3296–3299.
Wang, J., Dai, J., Xu, Y., Dai, X., Zhang, Y., Shi, W., Sellergren, B., Pan, G., 2018. Small. https://doi.org/10.1002/smll.201803913.
Wang, J., Qiu, H., Shen, H., Pan, J., Dai, X., Yan, Y., Pan, G., Sellergren, B., 2016b. Biosens. Bioelectron. 85, 387–394.
Wu, Z., Tao, C., Lin, C., Shen, D., Li, G., 2008. Chem 14 (36), 11358–11368.
Xue, F., Meng, Z., Wang, F., Wang, Q., Xue, M., Xu, Z., 2014. J. Mater. Chem. A 2 (25), 9559–9565.